Follow that Light: Leveraging LEDs for Relative Two-Dimensional Localization

Ander Galisteo
IMDEA Networks Institute &
Universidad Carlos III de Madrid
Madrid, Spain
ander.galisteo@imdea.org

Qing Wang
Delft University of Technology
Delft, the Netherlands
qing.wang@imdea.org

Aniruddha Deshpande
Delft University of Technology
Delft, Netherlands
a.deshpande@student.tudelft.nl

Marco Zuniga
Delft University of Technology
Delft, the Netherlands
m.a.zunigazamalloa@tudelft.nl

Domenico Giustiniano
IMDEA Networks Institute
Madrid, Spain
domenico.giustiniano@imdea.org

ABSTRACT

Visible light is gaining significant attention as a medium to achieve accurate relative localization. Most of the studies in the area focus on indoor positioning and rely on two important assumptions: (i) lights are *static*, and (ii) the receiver has line-of-sight with *multiple* lights. These requirements limit the application of localization methods in scenarios where nodes have a *single* light and are *mobile*, such as motorbikes or swarms of robots. In general, this particular type of scenarios (single lights moving on a plane) leads to underdetermined localization systems where no unique solution can be found. We follow a holistic approach that includes theory, simulations, and experiments to overcome *some* of the limitations present in such type of scenarios. Our theoretical and simulation results show that if nodes are enhanced with sensors providing relative directions (such as compasses), we can derive dependencies in the system to obtain unique solutions. Our proof-of-concept implementation validates our model by showing that single lights can provide relative localization with high accuracy: an average error below 5 cm.

CCS CONCEPTS

• **Networks → Mobile ad hoc networks**; • **Computer systems organization → Embedded systems**;

KEYWORDS

Visible light communication, Relative localization, Lambertian, Rotation, Analysis, Implementation, Evaluation

CoNEXT '17, December 12–15, 2017, Incheon, Republic of Korea

ACM ISBN 978-1-4503-5422-6/17/12…$15.00
https://doi.org/10.1145/3143361.3143371

ACM Reference Format:
Ander Galisteo, Qing Wang, Aniruddha Deshpande, Marco Zuniga, and Domenico Giustiniano. 2017. Follow that Light: Leveraging LEDs for Relative Two-Dimensional Localization. In *CoNEXT '17: The 13th International Conference on emerging Networking EXperiments and Technologies, December 12–15, 2017, Incheon, Republic of Korea.* ACM, New York, NY, USA, 12 pages. https://doi.org/10.1145/3143361.3143371

1 INTRODUCTION

During the last five years, there has been an increasing number of studies exploiting visible light for localization [5]. There are two main reasons for this trend: the pervasive presence of artificial lighting in our environments and the rather deterministic propagation properties of visible light waves, which makes them easy to model and predict [6].

Most of these studies focus on indoor positioning [2, 10]. Ceiling luminaries in our buildings and homes are seen as anchor points [14], and users with photoreceptors estimate their position based on the information obtained from nearby luminaries [7]. The strong focus on indoor positioning has lead many of these methods to make two important assumptions: (i) light sources are *static*, a realistic assumption given the fact that the location and orientation of most light fixtures are fixed in our ceilings; and (ii) users can expect *line-of-sight with many luminaries*, a stronger assumption that may not be always satisfied since it depends on the density of luminaries in the area and the Field-of-View (FoV) of the receiver.

While indoor positioning is justifiably considered the most relevant application of visible light methods, it may be valuable to remove the assumptions mentioned above, and extend these methods to other scenarios. In that manner, we could pave the way to create a new type of general localization methods that could be applied to *any* object (static or mobile) as long as it contains at least one LED light. This work is a step in such direction.

Scenario of interest. Consider two nodes, A and B, where node A would like to know the relative position of node B with respect to its position. These nodes could be any object containing a single light such as motorbikes or robots. Considering this scenario, our goal is the following: *as long as a node is within the illumination coverage of a neighbor, the node should be able to obtain its relative position without any prior knowledge of its surroundings.* These relative positions could be used for task coordination in the case of robots,

for vehicle-to-vehicle (V2V) and vehicle-to-infrastructure (V2I) communications in the case of smart vehicles, or can be leveraged by the beamforming techniques to increase the communication data rate.

Research problem. Localization methods based on visible light can be divided into two macro groups depending on the type of photoreceptor being used: cameras [4, 8] or photodiodes [19]. Cameras are a popular option but they have severe limitations decoding information at variable distances. Photodiodes (PDs), on the other hand, are known to operate well at a wide range of distances. Thus, our work focuses on PDs. The challenge of using phothodiodes is that the system needs to consider Lambertian radiation patterns. Several studies have looked into methods to exploit the properties of Lambertian patterns for localization [5, 9, 10]. Next we describe the key concepts we build upon from the state-of-the-art (SoA) and the novelty of our work.

Building Block 1: Inertial sensors. The first idea we build upon from the SoA is the use of inertial sensors. Contrary to isotropic sources, where a receiver can determine its unique *circular* iso-countour (locus in which every point satisfies the received power and orientation requirements) based on the received signal strength (RSS) observed from the transmitter, with LED sources the RSS information is not sufficient. To define a single *Lambertian* iso-contour the receiver needs information about its relative angle w.r.t. to the sender. To overcome this problem, several studies use accelerometers to determine the orientation of the receiver with respect to the ceiling [20], so a unique iso-countour can be defined per light. Then the iso-contours of several lights are used to localize the receiver (similar to standard trilateration methods). We also use inertial sensors to detect the direction of nodes, but we cannot use gravity as a frame of reference to derive orientations, because in our case lights are not fixed at ceilings.

Building Block 2: Rotations. The second idea we build upon from the SoA is the use of rotations to obtain more location information [18]. Without inertial sensors, receivers cannot pinpoint a unique iso-contour, but with inertial sensors receivers cannot only obtain their current iso-countour, but they can obtain more iso-countours by simply rotating on its same position. The reason for this phenomenon is that two different receiving angles create two different iso-countours. Note that with traditional isotropic sources rotations of the transmitter or receiver provide no extra information because the RSS remains the same. Rotation-based approaches have been used to add information (equations) to under-determined localization systems in order to obtain unique solutions. We also exploit rotations but considering more complex scenarios: rotations at the receiver, the transmitter or both. In traditional indoor settings only the simplest case is considered: rotations of the receiver.

Novelty: a localization framework for single mobile lights. Our key insight to map the traditional indoor localization problem to the mobile case is the following: *In the most general sense, mobility patterns involve changes in distance and direction*[1]*. Any change in direction –either by the transmitter, the receiver, or both– provides extra information to pinpoint the relative location of nodes, because for that short period of time (before and after the rotation), the distance between nodes could be assumed to be (roughly) the same.*

To achieve this goal, we assume that nodes have (i) a LED source, a compass sensor, and a photodiode (PD); and (ii) visible light communication capabilities, that is, nodes can modulate their lights to transmit information, and use their PDs to decode information. With these basic capabilities, our relative positioning algorithm works in the following manner. *First*, nodes use their lights not only for illumination but also to broadcast continuously information about three parameters: their direction (provided by the compass sensor), the light's output power (which determines the length of the beam) and the light's Lambertian order (which determines the width of the beam). *Then*, neighboring nodes use their PDs to decode the sender's information, and use our mathematical model to obtain its relative location based on (i) the information received from the sender, (ii) its own direction and (iii) the detected signal strength.

Our contributions. Considering the above mentioned challenges the key contributions of our work are:

- Method [Sections 4 and 5]. We derive closed-form expressions to obtain unique localization solutions for cases where either the transmitter or the receiver rotate. For the case where both nodes rotate, we show that multiple solutions are possible, but we use simulations to provide some basic rules that help with identifying a single solution.
- Evaluation [Sections 6 and 7]. We implement our model with off-the-shelf components and perform a systematic evaluation of our approach. We analyze the effects of single and concurrent rotations and perform evaluations with mobile nodes. Our results show that our method can provide localization errors below 5 cm.

2 MAIN CONCEPT

In this section, we present background information to understand the concept of Lambertian patterns and the basic localization principle behind this work.

2.1 Lambertian patterns

Consider an LED light source (transmitter) and an optical receiver, as illustrated in Fig. 1. Given any output power at the transmitter (LED), the received signal strength at the receiver (PD) depends on three key parameters: the distance between them (d), the irradiation angle (ψ) and the incidence angle (θ). The longer the distance, or the wider any of these angles, the lower the received signal strength (RSS). The interplay among these three parameters leads to Lambertian radiation patterns, where the maximum length of the coverage is mainly determined by the output power of the LED and the maximum width is determined by the Lambertian order (m). A small value of m leads to a broad coverage of the LED; a large m leads to a long but narrow coverage.

Formally, this pattern is captured by the well-known Lambert's cosine law [6]:

$$R_t(\psi) = \frac{m+1}{2\pi}\cos^m(\psi) \quad (1)$$

[1]This is the highest level of abstraction used by one of the most popular mobility models: the random way-point model.

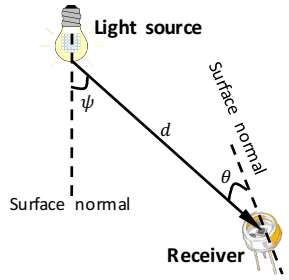

Figure 1: Propagation properties of LEDs

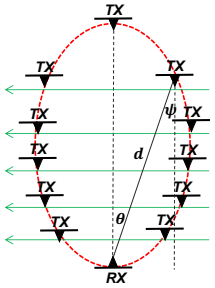

Figure 2: Iso-contours of received power

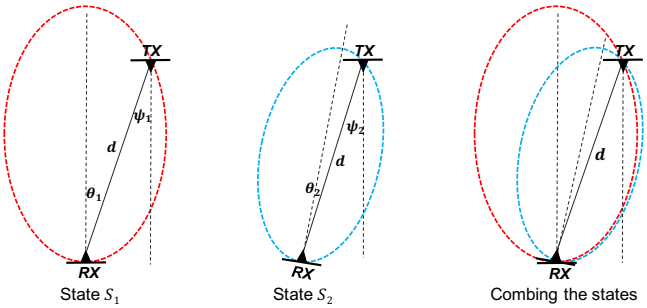

Figure 3: Localization using iso-contours intersection

The channel loss $H(0)$ between the transmitter and receiver is

$$H(0) = \begin{cases} A_{\text{RX}} \cdot \frac{m+1}{2\pi d^2} \cos^m(\psi) \cos\theta & \text{for} \quad \theta \in [0, \Theta_c], \\ 0 & \text{for} \quad \theta > \Theta_c \end{cases} \tag{2}$$

where A_{RX} is the sensing area of the photodiode (PD) of the receiver, and Θ_c is the PD's Field-of-View (FoV).

Letting P_t and P_r denote the optical transmission power of the LED and the received power at the PD, respectively; and letting N refer to the sum of ambient noise and the PD's shot and thermal noise; then P_r can be written as:

$$P_r = P_t \cdot H(0) \cdot g_r(\theta) + N \tag{3}$$

where $g_r(\theta)$ is the optical gain of the PD. $g_r(\theta)$ is a non-zero *constant* when $\theta \in [0, \Theta_c]$, and is zero otherwise [21]. Therefore, in the rest of this paper, we simply use g_r to denote $g_r(\theta)$ in the calculation of P_r.

2.2 Basic localization principle

Given a received power P_r, the TX can be present in multiple positions with respect to the RX, cf. Eq. (2). For example, for a low P_r, the TX can be far away but aligned to the RX ($\psi = \theta = 0$), or it can be nearby but misaligned. If we fix the TX's orientation and move it in a horizontal 'scanning' motion at different perpendicular distances from the RX, as illustrated in Fig. 2, each scan provides two locations where the received power is measured as P_r. All these locations form an *iso-contour* where the received power is the same.

The principle behind this work is to exploit changes in the iso-contours due to nodes' movements, cf. Fig. 3. If the RX rotates, the iso-contour changes from its original shape (red) to a new shape (blue). In this particular case, the change in the iso-contour is caused by the change in the incidence angle θ. The intersection of these two iso-contours can be used to estimate the relative position of the TX. In this work, we exploit this property in *mobile scenarios*, where any type of node, TX or RX, can move freely.

3 SYSTEM MODEL

Consider a system of two *mobile* nodes: one acts as a reference point (referred as receiver) that has a PD; and the other is a target to be localized (referred as transmitter) that has an LED light source. Both nodes can measure their orientations and movement through on-board sensors, compasses and accelerometers respectively. The transmitter has information of the optical properties of its LED lights, such as the transmission power and Lambertian order. The transmission power and Lambertian order together with the transmitter's real-time orientation are shared with the receiver via visible light communication. The receiver can decode the transmitted information through its PD and it can also measure the received power.

Next we define the *state* of our system. Since we assume that both nodes are mobile, we define a state S as follows:

$$S = (\alpha_{\text{tx}}, \alpha_{\text{rx}}, d, P_r) \tag{4}$$

where α_{tx} and α_{rx} are the orientations of the transmitter and receiver with respect to North, respectively, d is the relative distance of the transmitter with respect to the receiver, and P_r is the received power at the receiver.

As discussed in Sec. 2.2, given fixed positions and orientations of the transmitter and receiver, there exists an iso-contour for the received power P_r. But we need more than one iso-countour to pinpoint a unique location. The problem we face in our scenario is two-fold. First, for the iso-contours to be useful, we need them to be rooted at the same location, but given that we are dealing with mobile nodes each iso-countour could be rooted at different locations, rendering the information useless for our localization process. Second, we face an under-determined system, where we have many variables but not enough equations.

Let us describe our second challenge in a more formal manner. Assume our system is currently in state $S_1(\alpha^1_{\text{tx}}, \alpha^1_{\text{rx}}, d_1, P^1_r)$. According to Eq. (3), the received power P^1_r for state S_1 can be written as follows:

$$P^1_r = P_t A_{\text{RX}} \frac{m+1}{2\pi (d_1)^2} \cos^m(\psi_1) \cos(\theta_1) \cdot g_r + N \tag{5}$$

A similar equation can be derived for a later state $S_2(\alpha^2_{\text{tx}}, \alpha^2_{\text{rx}}, d_2, P^2_r)$, where the relative position and the orientations of the transmitter and receiver change, and are denoted by d_2, α^2_{tx}, and α^2_{tx}, respectively; and the measured received power is P^2_r:

$$P^2_r = P_t A_{\text{RX}} \frac{m+1}{2\pi (d_2)^2} \cos^m(\psi_2) \cos(\theta_2) \cdot g_r + N \tag{6}$$

In the above two equations, we have six variables: the irradiation angles ψ_1, ψ_2, the incidence angles θ_1, θ_2, and the relative distance d_1 and d_2 between the transmitter and receiver. So we can not solve them directly.

To overcome the aforementioned challenges we propose two approaches. First, we force nodes to broadcast continuously and periodically their orientation and LED parameters via visible light

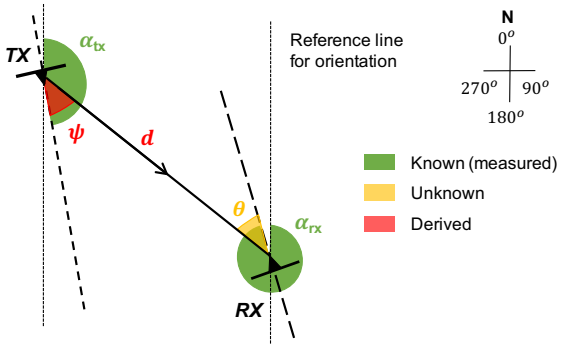

Figure 4: Relation between irradiation angle, incidence angle, and orientations

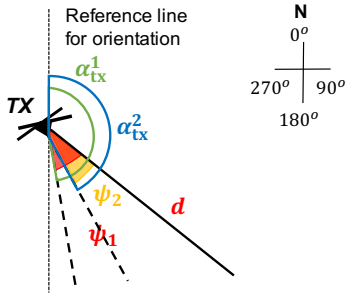

Figure 5: Relation between irradiation angles.

communication. And, at the receiver, we only consider changes in orientation detected within a very short period of time, so we can assume that the locations of the TX and RX remain "constant". This approach has two important consequences, first it allows us to assume that the two iso-countours are rooted at the same point; and second, it reduces the number of variables in the above equations from six to five, because over a short period of time we can assume that $d_1 = d_2 = d$. Second, we exploit the information coming from the compasses to derive dependencies among the five remaining variables, enabling us to identify a single solution in most cases.

4 ANALYSIS

In this section we derive the dependencies that exist among the unknown variables described in Eqs. (5) and (6). Our analysis focuses on changes in orientations, but we also provide some results for scenarios where there are no changes in orientations but there are changes in distance, for example, two mobile nodes in a straight road moving at variable speeds.

4.1 Deriving dependencies

For these derivations, we consider a short period of time where the relative distance between the transmitter and receiver is 'fixed' while their relative orientations change.

First, we will identify dependencies for the incidence angles, which will remove two unknowns (θ_1 and θ_2). The incidence angles θ_i are a function of the orientations of the TX and RX as well as the irradiation angles ψ_i. Considering states S_1 and S_2, these dependencies can be described as follows.

Dependency 1: $\theta_1 = f(\alpha^1_{tx}, \alpha^1_{rx}, \psi_1)$

Dependency 2: $\theta_2 = f(\alpha^2_{tx}, \alpha^2_{rx}, \psi_2)$

This relationship is illustrated in Fig. 4. Let $\Delta\alpha^i$ be the relative angle between the orientations of the RX and TX at state S_i, then we have

$$\Delta\alpha^i = \alpha^i_{rx} - \alpha^i_{tx}, \quad i \in [1, 2] \tag{7}$$

Further, the incidence angle θ_i can be expressed as:

$$\theta_i = \pi + \psi_i + \Delta\alpha^i = -\pi + \psi_i + \alpha^i_{rx} - \alpha^i_{tx}, \quad i \in [1, 2] \tag{8}$$

Second, we will identify a dependency for the irradiation angle ψ_2, which will remove one extra unknown. The irradiation angle ψ_2 is a function of the irradiation angle ψ_1 and the orientations of the TX in both states:

Dependency 3: $\psi_2 = g(\alpha^1_{tx}, \alpha^2_{tx}, \psi_1)$

This dependency is illustrated in Figure 5. Let $\Delta\alpha_{tx}$ be the difference of the TX's orientations in states S_1 and S_2, then

$$\Delta\alpha_{tx} = \alpha^2_{tx} - \alpha^1_{tx} \tag{9}$$

Based on this, we can derive the expression of ψ_2 as follows:

$$\psi_2 = \Delta\alpha_{tx} + \psi_1 = \alpha^2_{tx} - \alpha^1_{tx} + \psi_1 \tag{10}$$

Finally, substituting the above three dependencies into Eq. (5) and Eq. (6), we have

$$P^1_r = P_t A_{RX} \frac{m+1}{2\pi d^2} \cos^m(\psi_1) \cos(f(\alpha^1_{tx}, \alpha^1_{rx}, \psi_1)) \cdot g_r + N \tag{11}$$

$$P^2_r = P_t A_{RX} \frac{m+1}{2\pi d^2} \cos^m(g(\alpha^1_{tx}, \alpha^2_{tx}, \psi_1)) \cos(f(\alpha^1_{tx}, \alpha^2_{tx}, \alpha^1_{rx}, \alpha^2_{rx}, \psi_1)) \cdot g_r + N \tag{12}$$

In these two equations there are only two unknowns (ψ_1 and d), and thus, they can be solved numerically. Next, we will describe how to solve these functions for two cases: non-simultaneous and simultaneous rotations. We define *simultaneous* rotations as those events where both, the TX and RX, change their orientations within the same short period of time. If the changes of orientations occur in different periods, we consider the rotations to be non-simultaneous. Notice that our definition depends on how often we send up-to-date information over the visible light channel. For our implementation, simultaneous rotations are those occurring within 2 ms of each other (due to the sampling rate of our sensors).

4.2 Non-simultaneous rotations

We will first consider the scenario where the RX rotates, and then, we will consider the scenario where the TX rotates. The first scenario is simpler and is the one we find in indoor setups (because the lights, TXs, are fixed).

1) RX rotates. For the scenario where the RX rotates, we have the following proposition.

Proposition 4.1. *If the RX rotates and the TX is fixed, i.e., TX does not rotate between the two states S_1 and S_2, then we have the*

following closed-form expression of θ_2:

$$\theta_2 = \arctan\left(\frac{(P_r^1 - N)\cos(\alpha_{rx}^2) - (P_r^2 - N)\cos(\alpha_{rx}^1)}{(P_r^1 - N)\sin(\alpha_{rx}^2) - (P_r^2 - N)\sin(\alpha_{rx}^1)}\right) - \pi + \alpha_{rx}^2 \tag{13}$$

Proof. The proof is presented in Appendix A.1. □

2) TX rotates. For the scenario where the TX rotates, the analysis is different from the scenario where the RX rotates. This occurs because the path loss caused by the TX is magnified by the Lambertian order m: $\cos^m(\psi)$, cf. Eq. (2), whereas the path loss caused by the RX is not ($\cos(\theta)$). Therefore, for $m > 1$ (which are common Lambertian orders for most LEDs), the same rotation angle at the TX and the RX will have a different impact. For the scenario where the TX rotates, we have the following proposition.

Proposition 4.2. *If the TX rotates and the RX is fixed, i.e., RX does not rotate between the two states S_1 and S_2, then we have the following closed-form expression of θ_2:*

$$\theta_2 = \arctan(j) - \pi + \alpha_{rx}^2 - \alpha_{tx}^1 \tag{14}$$

where

$$j = \frac{\cos(\alpha_{tx}^2 - \alpha_{tx}^1) - \sqrt[m]{\frac{(P_r^2 - N)}{(P_r^1 - N)}}}{\sin\left(\alpha_{tx}^2 - \alpha_{tx}^1\right)}$$

Proof. The proof is presented in Appendix A.2. □

For both non-simultaneous rotations, we have closed-form expressions for θ_2. Thus, we can obtain *the closed-form expression of the distance d* based on Eq. (11) and (12):

$$d = \sqrt{\frac{(m+1)A_{\text{RX}}}{2\pi(P_r^1 - N)}\cos^m(\psi_1)\cos(\psi_1 - \pi - \alpha_{\text{tx}}^1 + \alpha_{\text{rx}}^1)\cdot g_r}$$

Based on the closed-form expressions of θ_2 and d, we obtain the relative position of the TX with respect to the RX, and thus, we can conclude that for non-simultaneous rotations, we have *unique* solutions to Eq. (11) and (12).

4.3 Simultaneous rotations

For these scenarios, we are not able to derive closed-form expressions for θ_2 and d. This is due to the fact that the transmission pattern is Lambertian with the form $\cos^m(\cdot)$ where m is positive and real. We can only solve the equations numerically. Based on Eq. (11) and (12), we first derive an equation where ψ_1 is the only unknown variable.

Proposition 4.3. *By transforming the problem from the ψ_1 domain to the k domain, we have the following polynomial expression for k:*

$$b \cdot \sin(h) \cdot k^{m+1} + b \cdot y \cdot k^m - \sin(c) \cdot k - x = 0 \tag{15}$$

where k is a function of ψ_1:

$$k = \cos e - \tan(\psi_1) \cdot \sin e \tag{16}$$

and

$$\begin{cases} b = \frac{P_r^1 - N}{P_r^2 - N} \\ c = \alpha_{rx}^1 - \alpha_{tx}^1 \\ e = \alpha_{tx}^2 - \alpha_{tx}^1 \\ h = \alpha_{rx}^2 - \alpha_{tx}^1 \\ x = \sin(\alpha_{tx}^2 - \alpha_{rx}^1) \\ y = \sin(\alpha_{tx}^2 - \alpha_{rx}^2) \end{cases}$$

Proof. The proof is presented in Appendix A.3. □

Proposition 4.3 implies that by solving the polynomial in Eq. (15), we can get all possible solutions for k; and once k is known, we can use Eq. (16) to obtain:

$$\theta_2 = \arctan\left(\frac{\cos e - k}{\sin e}\right) - \pi + \alpha_{rx}^2 - \alpha_{tx}^1 \tag{17}$$

And d can be obtained by substituting Eq. (17) into Eq. (15).

From Eq. (15) and (17) we observe that we can have up to $m + 1$ solutions for our localization problem. However, by considering some physical constraints such as the FoVs of the TX and the RX, we can filter out some of the results. We will look further into this issue in Sec. 5.

4.4 Impact of measurement errors

Based on the dependencies derived earlier in this section, we now analyze the effects of measurements errors in our system. We focus on orientation errors (α_{rx} and α_{tx}) and errors in the received power (P_r).

From Eq. (12), we can derive the distances d as a function of the other parameters:

$$d^2 \propto \frac{\cos^m(\psi_1)\cos(f(\alpha_{\text{tx}}^1, \alpha_{\text{rx}}^1, \psi_1))}{P_r^1}$$

$$d^2 \propto \frac{\cos^m(g(\alpha_{\text{tx}}^1, \alpha_{\text{tx}}^2, \psi_1))\cos(f(\alpha_{\text{tx}}^1, \alpha_{\text{tx}}^2, \alpha_{\text{rx}}^1, \alpha_{\text{rx}}^2, \psi_1))}{P_r^2}$$

Based on these equations, we derive the following insights:

Insight 1: Lights with wider beams ameliorate the effect of orientation errors in the TX. Given an error in the orientation of the TX, a wider beam (small m) will lead to more accurate location estimations than a narrower beam (large m). This occurs because the cos() function takes values between 0 and 1. If the Lambertian order is high (narrow LED beam), the error will be exacerbated because it will be elevated to a power m. Thus, for mobile scenarios, Lambertian sources with $m = 1$ are the preferred choice. Note that in indoor scenarios this is a lesser problem because lights are fixed to the ceiling, and thus, the orientation is known and fixed.

Insight 2: Orientation errors at the RX are more detrimental when the RX lies at the edges of the illumination area. Errors on the RX's orientation will have a particularly negative impact as the RX moves away from the normal surface of the transmitter. This occurs because the cos() function decreases rapidly as the incidence angle moves away from 0^o. Thus, the more aligned the TX and RX are, the higher the accuracy of our estimations.

Insight 3: Measurement errors in the received power will have a larger effect at longer distances. This is a property that is common to all

electromagnetic sources because the intensity decays exponentially with distance. Thus at close distances, errors in P_r will lead to small errors in localization, but at longer distances the same error in P_r can lead to exponentially larger errors in localization.

4.5 Variable distances

Until now, our analysis has focused solely on events where rotations are expected. But some mobile scenarios may not have any rotations. For example, nodes moving on a straight path at variable speeds will not change their orientations, but their relative distances will change. For these types of scenarios, the equations describing the system at states S_1 and S_2 are

$$P_r^i = P_t A_{\text{RX}} \frac{m+1}{2\pi d_i^2} \cos^m(\psi) \cos(\theta) + N, \quad i \in \{1, 2\} \tag{18}$$

If we assume that we can estimate the difference in distances between states S_1 and S_2 (by for example performing a double integral of an accelerometer):

$$\varepsilon = d_2 - d_1 \tag{19}$$

Then, based on Eq. (18) and Eq. (19), we can obtain a closed-form expression for the relative distance as follows:

$$d_2 = \frac{\varepsilon}{1 - \sqrt{\frac{P_r^2}{P_r^1}}} \tag{20}$$

From Eqs. (20), (8), and (18), we have the following expression

$$\frac{2\pi d_2^2 P_r^2}{(m+1)A_{\text{RX}}} - N = \cos^m(\theta + \pi + \alpha_{tx} - \alpha_{rx}) \cos(\theta) \tag{21}$$

where θ can be calculated numerically.

An important point to consider for these no-rotations cases is that the relative location is no longer obtained by intersecting two Lambertian iso-contours, but by intersecting a single Lambertian iso-contour and a circle. This implies that unless the TX and RX are aligned ($\psi = \theta = 0$), we will always obtain two possible locations. Nevertheless, due to physical restrictions in the system in practical, one of the location could be discarded.

5 MODEL VALIDATION AND INSIGHTS FOR THE DESIGN

In this section, we perform extensive simulations to validate the models in Sec. 4 and provide significant insights in the design of the systems. For each scenario, the values of ψ_1, ψ_2, θ_1 and θ_1 are randomly chosen following a uniform distribution between $\frac{-\pi}{2}$ and $\frac{\pi}{2}$. The maximum *coverage* distance between a TX and RX is then computed by taking into account that the maximum path loss can be 20 dB (beyond that threshold no communication can be reached). We perform 10,000 simulations per scenario.

Based on Eqs. (5) and (6), in what follows, we call *iso-contour* the shape that represents all the possible positions that the receiver could be, given some values of α_{tx}^i, α_{rx}^i and P_r^i. The iso-contour shape contains two main components:

- The component relative to the transmitter ($\cos(\psi_i)^m$).
- The component relative to the receiver ($\cos(\theta_i)$).

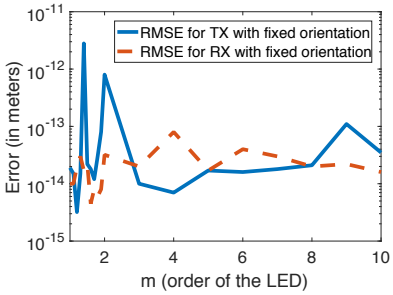

(a) Model validation (RMSE of the positioning error between model and simulation).

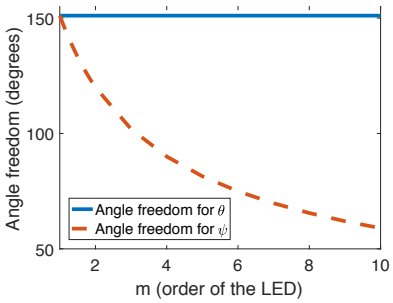

(b) Angle freedom over m.

Figure 6: (a) model validation when either the transmitter or the receiver is fixed (non-simultaneous case). (b) angle freedom for θ (blue) and ψ (orange) for different values of m.

After a rotation or a distance change (see previous section), a new iso-contour is generated. Each point (2D coordinates) where both iso-contours cross is the result returned by the algorithm.

Based on these considerations, in what follows we present our study for the different setups, starting with the non-simultaneous rotations case.

5.1 Non-simultaneous rotations

To validate Proposition 4.1 and Proposition 4.2 (non-simultaneous cases), we perform a brute-force study in a noiseless scenario. We then compute the root mean square error (RMSE) of the position error varying m. The results are presented in Fig. 6(a). The figure shows that the RMSE is less than 10^{-11}, regardless of m (this error is due to the computational limits of the simulator). This shows that the models for non-simultaneous scenarios are correct. In addition, we always find one unique solution of the system. This is expected, as two Lambertian iso-contours generated from the same source with a different rotation angle can only cross in one point in space.

Due to the directionality of LEDs, rotating the transmitter will have a much higher impact on the received power than rotating the receiver. The difference increases with m. In order to confirm this, we place the transmitter and the receiver at half the distance from the maximum coverage distance for the configured sensitivity. We then rotate the transmitter until the received signal is below the sensitivity threshold. Afterwards, the same is done at the receiver.

The range of angles where the received power is above the sensitivity threshold is called angle freedom. Fig. 6(b) shows that, while the angle freedom remains constant for the receiver, it decreases for the transmitter as m increases. This confirms that rotations in the transmitter are more critical than at the receiver.

5.2 Simultaneous rotations

We now study Proposition 4.3 for the simultaneous scenario. Unlike the non-simultaneous case, in this case both transmitter and receiver are free to rotate. Solving Eq. (15), we may get either a unique solution or more than one solution, depending on m. From a physical point of view, both components $\cos(\psi_i)^m$ of the transmitter and $\cos(\theta_i)$ of the receiver change, and thus the shape of the iso-contour changes, making *several* results possible. But for location purposes, it is desired to have only *one* solution.

Next we show that we can follow some basic rules to discard many potential solutions to reach (in most cases) a single solution. Some solutions can be discarded as follows: i) discard solutions that give complex numbers, ii) discard solutions with no physical meaning, iii) discard solutions unlikely to happen in real environments.

For natural m, as it can be seen in Fig. 7(a) and as expected from Eq. (15), the number of possible solution that can be computed numerically increases with m. Nevertheless, the number of maximum real solutions, and thus with a physical meaning, is three or four depending on m. Intuitively, the fact that maximum number of real solutions is four, can be explained by the fact that two concave surfaces intersect in at most four points.

The next physical constraint that can be introduced into the system is that ψ_1, ψ_2, θ_1 and θ_1 need to be between $-\frac{\pi}{2}$ and $-\frac{\pi}{2}$. If any of them is not, the communication would not have been possible, because that will require the transmitter (in the case of ψ) or the receiver (in the case of θ) to have transmitted or received with the back of the LED or the photodiode, respectively, so the solution could be discarded.

Finally, the last restriction that has been introduced in the system is the distance restriction. It is assumed that the distance is not going to be very short (less than 1cm), so solutions that lay inside this region are discarded too.

An analysis on how the aforementioned constraints affect the number of possible solutions is performed, and the results are shown in Fig. 7(b). If we do not apply our constraints, the number of scenarios with unique solutions is low. But when we take into consideration the constraints we derived, the number of scenarios with unique solutions go from around 30% to close to 70%.

5.2.1 Measurement error. Finally, we study how errors in the compass readings affect the system. For this study, we assume a Gaussian noise with $\sigma = 5$ for both TX's and RX's compasses[2]. The RMSE of the distance is in the order of 10^{-1} meters, which means accuracy of decimeters. The accuracy of the TX's orientation is the key to minimize the error as the TX is more directional than the RX. Comparing the two non-simultaneous scenarios, it can be seen that when we fix the TX's orientation, the error is 50% smaller than when we fix the RX's orientation. The error in the simultaneous scenario is comparable to the worst error in the non-simultaneous scenario. These results highlight an important difference between our work and the SoA, which focus on indoor scenarios where the TXs are fixed, and thus are less challenging.

[2]This value of σ characterizes the effect of buildings on compass errors [13]. Outdoors the errors in compass are far lower.

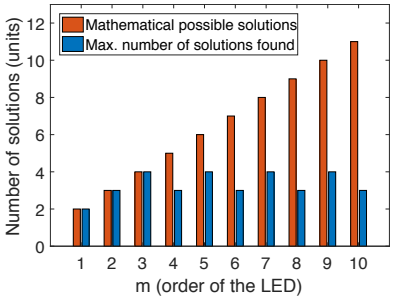

(a) Total vs real solutions varying m.

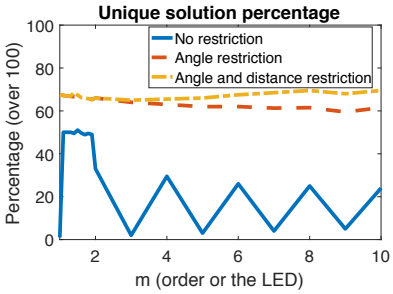

(b) Unique solutions.

Figure 7: (a) number of mathematically possible solutions and number of real solutions through numerical analysis. (b) percentage of unique solutions with and without physical constraints.

5.2.2 Insights. First, we observe that a compromise is needed when choosing the order m of the LED. A small m implies a wider covered area (good), smaller power distributed in the direction of maximum emission (not good) and a slightly smaller number of real solutions considering physical constraints (good). The opposite holds when increasing m. Second, it is preferable to have mobility patterns where the receiver is the one rotating. This is due to the fact that LEDs have Lambertian sources and rotation in transmitters may cause larger power received differences. Finally, in the simultaneous scenario, it may be desirable to have more than two measurements. In this way, several results may be discarded and the one common result should remain as the correct one.

5.3 Variable distances

We verify the correctness of the closed-form expression for fixed angle introduced in Eq. (20). For this study, we compute the position considering a brute force analysis varying m. The RMSE in distance between the simulated position and the one computed by the model is below 10^{-12} for 100% of the time (the difference is due, as above, to computational limitations), that confirms the correctness of the model.

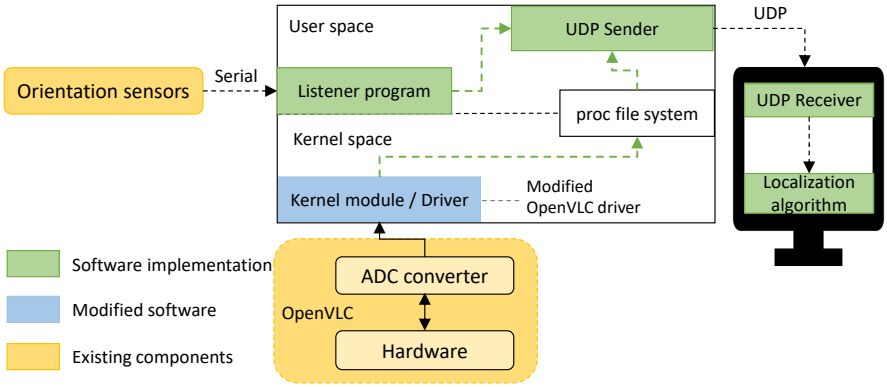

Figure 8: Functional blocks of our system

6 IMPLEMENTATION

We implement our localization algorithm in the OpenVLC platform [15, 16] for low-cost Visible Light Communication (VLC). OpenVLC consists of three parts: a BeagleBone Black (BBB) board, an optical front-end transceiver and the software solution. We customize it to satisfy the requirements of our localization method. The functional blocks of our system are shown in Fig. 8. As indicated in Eq. (12), to run our localization method, we need the following information from the TX: *transmitted power, Lambertian order m of its transmitting LED and its orientation.* And the following information from the RX: *received power and its orientation.*

Measuring the orientation of nodes. Orientation plays a crucial part in our system and it can be measured by inertial sensors. The sensor used is *Adafruit 9-DOF Absolute Orientation IMU Fusion Breakout - BNO055*, which does sensor fusion of the magnetometer and accelerometers for higher accuracy. Our OpenVLC node communicates to the sensor using the serial port, as shown in Fig. 9. The sampling rate of the sensors is equal to 500 Hz.

Sharing information between nodes. *The transmission power, Lambertian order of the LED at the TX, and the TX's orientation* must be shared with the RX. In our work, we use visible light communication to achieve this. We modify the original frame format of OpenVLC by adding three fields to convey this information, as shown in Table 1.

Calculating the received power. The preamble of each frame is used to determine the received power. The length of the preamble is 24 bits (cf. Table 1). These bits are composed of alternate HIGH and LOW symbols, primarily used for synchronization. Information pertaining to the received power can be extracted based on the preamble. We measure P_r for each HIGH symbol. The measurement comprises the total power received from the LED plus ambient noise and PD's shot and thermal noise (cf. Eq. (3)). In order to have controlled environment for our evaluation, measurements are done in a dark environment without external light sources.

Table 1: Modified frame format in our system

Preamble	...	*Transmission power*	*Lambertian order*	*Orientation*	...
3 Bytes	...	*1B*	*1B*	*2B*	...

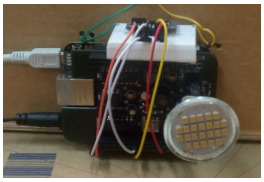

Figure 9: Sensors connected through serial to the BBB, and the BBB to the computer via USB

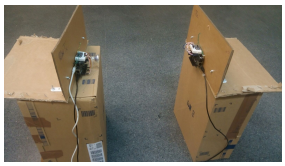

Figure 10: A snapshot of the experiment setup

Localization. The localization algorithm is implemented to operate in real time, with interactions among the blocks illustrated in Fig. 8. First, we modify the OpenVLC driver to collect raw power readings from the data frame preamble, and share these readings with the user space using the *proc* file system. Second, a listener program collects the orientation information from sensors by continuously polling the serial port in the Beaglebone board. The listener thread then sends the data to the computer every second using UDP. In the computer, a program reads the UPD messages and every two messages, runs the localization algorithm based on Eq. (12).

7 EXPERIMENTAL EVALUATION

We evaluate the proposed relative localization method with experiments under various settings. When the LED emits the symbol HIGH, it is supplied at a voltage of 12 V. The measured current (in general, depending on the LED characteristics) is equal to 52 mA. This results in a total power emitted by the LED close to 0.6 W (some power in the order of 0.1-0.2 W is dissipated by the driving circuit). The PD used at the RX is the OPT101[3]. A snapshot of the experiment setup is shown in Fig. 10. The system is located in a 15.2×5.8 meter empty room, which is dark (<3 lux). The TX and RX are located at a sufficiently high distance from the ground to minimize reflections from the floor. In all the tests, the RX is located in the position $(0, 0)$ while the transmitter is placed in different locations.

[3]http://www.ti.com/lit/ds/symlink/opt101.pdf.

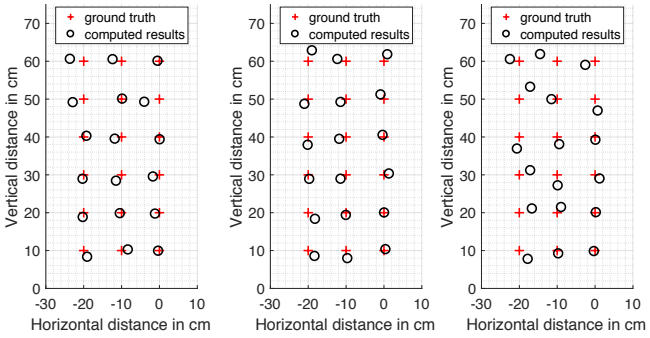

(a) Only RX rotates (b) Only TX rotates (c) Both rotate

Figure 11: Accuracy results for rotations

Next, we first characterize the system and then we evaluate our localization method in several key scenarios.

7.1 System characterization

The first step is to characterize the system for our particular hardware. From Eq. (5), we observe that the values we need to characterize are m, A_{RX}, and g_r.

7.1.1 m calculation. Dividing Eq. (5) and Eq. (6), configuring $\theta = 0$ and knowing ψ_1 and ψ_2 we get the following expression:

$$m = \frac{\log\left(\frac{Pr_1}{Pr_2}\right)}{\log\left(\frac{\cos(\psi_1)}{\cos(\psi_2)}\right)} \tag{22}$$

The value of m has been computed for different values of ψ_1 and ψ_2 and the average is taken as the final value, which leads to $m = 1$. Following the insights from the previous sections, the use of an LED with low m has several benefits and the only drawback of reduced sensitivity in the direction of maximum light emission. The maximum communication range in our setup is of approximately 1 meter, when the transmitter and receiver are perfectly aligned. The range could be increased with LEDs of higher nominal power and with more sensitive photodiodes.

7.1.2 A_{RX} and g_r calculation. For a single measurement, $A_{\text{RX}} \cdot g_r$ can be calculated as:

$$A_{\text{RX}} \cdot g_r = \frac{2\pi d^2}{(m+1) \cdot \cos^m(\psi_1) \cdot \cos(\theta_1) \cdot P_r^1} \tag{23}$$

The system is measured for several values of d so that ψ_1 and θ_1 are 0. The average value of $A_{\text{RX}} \cdot g_r$ is 20902.

7.2 Relative angles variation

We consider three scenarios: TX rotation, RX rotation or both. The rotation angles both for transmitter and receiver are (0, 20, 30, 45, 60, -20, -30, -45, -60) degrees and the real locations of the transmitter in cm units are equal to (0, -10, -20) for x and (0, 10, 20, 30, 40, 50, 60) for y.

The results of all these experiments are shown in Fig. 11 and a summary of the average error is presented in Table 2. They show an average error in the x- and y-axis of less than 3.5 cm for all the cases, resulting in a position error of less than 5 cm. Position errors could be caused, in part, by small errors in the estimation of the Lambertian order m that has been performed manually (cf. Eq. (22)). More accurate values could be either available in datasheets of professional LEDs or measured through advanced photometers tools.

Table 2: Mean error in the x- and y-axis for rotations.

	Mean x-axis error	Mean y-axis error
Only RX rotates	2.61 cm	1.63 cm
Only TX rotates	3.20 cm	2.11 cm
Both rotate	3.83 cm	3.47 cm

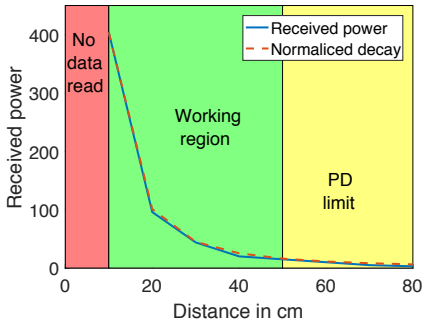

Figure 12: Real received power and theoretical distance decay over distance.

It can be also seen than the error increases with the distance (Insight 3 in Section 4.4). This occurs because the sensitivity of the photodiode affects more the results when the received signal is closer to the receiver's noise. An illustration of this phenomenon is presented in Fig. 12. Another problem of photodiodes is that we cannot distinguish well scenarios with very short distance (less than 10 cm in our experiments) as photodiodes get saturated. However, a more advanced receiver can reduce the impact of this issue.

For the case of both devices rotating, it must be noted that the number of solutions we find is two for all the configurations. This is expected from Fig. 7(a) and the selection of Lambertian order close to $m = 1$. Nevertheless, one of the solutions could always be discarded because it belongs to a scenario where no transmission could be accomplished (cf. Section 5). The discarded solution requires the receiver to be in an invalid orientation with respect to the transmitter.

7.3 Relative distance variation

In these experiments both the TX and RX are free to move assuming that they do not change their orientation with respect to each other. In order to compute the correct value of the system, the distance difference needs to be known as well as the received power. In these experiments the distance change is assumed to be known (in a real system it can be estimated with a double integration of the accelerometer input).

In the experiments, the distance between the TX and RX changes between the first and the second measurement with different steps (10, 20, 40, 50 cm). This is performed for different angles in degrees

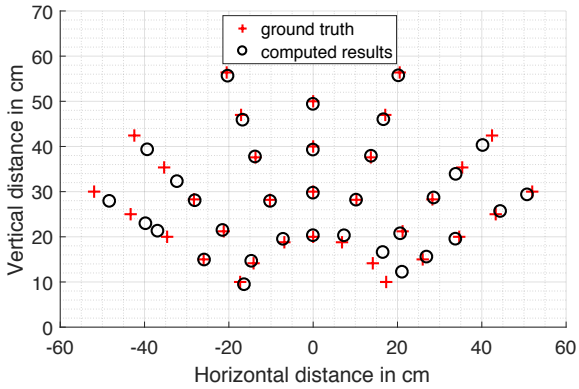

Figure 13: Accuracy results for distance changes.

Table 3: Mean error in the x- and y-axis for distance changes

	Mean x-axis error	Mean y-axis error
Distance change	1.65 cm	1.13 cm

between the TX and RX (0, 20, 45, 60, -20, -45, -60). The results of the experiments are depicted in Fig. 13 and the average distance error in the x- and y-axis are shown in Table 2. The table shows a small position error (less than 2 cm) which validates the accuracy of our system.

It is important to mention that the system returns a second different solution around 25% of the time. This is due to the specific configuration of the system that allows, mathematically, more than one solution. Nevertheless, once the angle restrictions derived in Section 5 are applied, the solution remained unique for all the experiments.

7.4 Full mobile case

In this last scenario both nodes (i.e., the TX and RX) are free to move and orient themselves in any direction (within the FoV of each other). We conduct experiments by moving both nodes on tracks as shown in Fig. 14(a-b) to simulate the movements of robots or vehicles on a road. The localization is performed whenever the TX is at a reference position (marked in red color). We note that for straight paths like Track 1, ideally there are no changes in orientation of the nodes. However, even minor changes in the orientation are useful and exploited by our system. The localization results are shown in Fig. 14(c-d). The estimated localized positions of the RX are marked with blue squares. We observe that the results are quite accurate, with a maximal error of around 2 cm.

This approach works because the sampling rate and data communication are sufficiently fast to assume that the distance does not change between two consecutive samples.

8 RELATED WORK

Localization has been studied widely [11]. Here we focus our discussion on studies leveraging methods based on visible light. Table 4

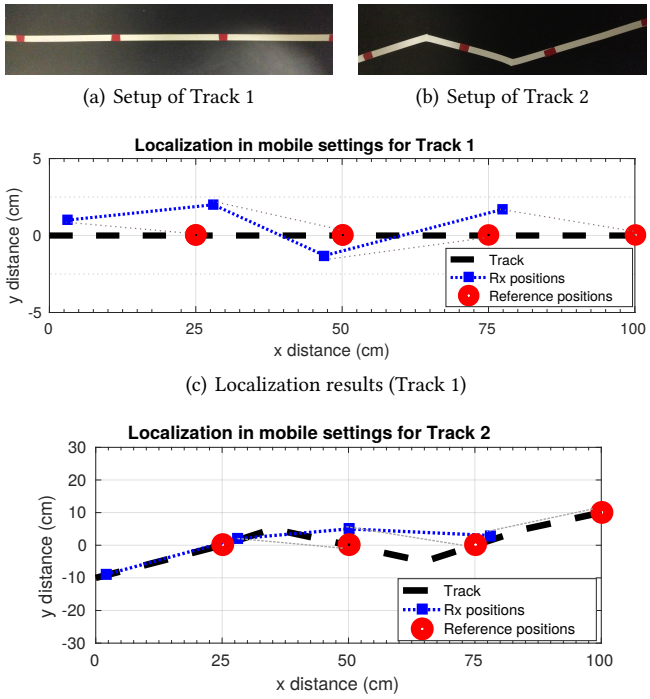

(a) Setup of Track 1 (b) Setup of Track 2

(c) Localization results (Track 1)

(d) Localization results (Track 2)

Figure 14: Accuracy results for fully mobile case.

positions the novelty of our work within the most relevant studies in the SoA.

Initially, most visible light positioning solutions were built based on existing radio-frequency techniques [10], borrowing concepts such as proximity [3] and fingerprinting [14]. A second generation of methods then started to exploit the unique properties of light, such as the free-space optical propagation property and the limited multi-path [5]. In this category of works, at least three Lambertian LED sources are required to achieve high accuracy using multilateration algorithms [9]. Other schemes exploit the difference in attenuation between signals received from LED pairs to estimate distances [12], but they require a high modulation rate as well as an increased installation cost to synchronize the LEDs. Camera/vision-based positioning has also been studied in the context of smartphones acting as receivers [8, 22]. Most studies rely on intensity modulation, but polarization-based modulation has been also considered for wearable applications [17]. Other works use legacy light fixtures such as fluorescent lights [22, 23] to provide indoor localization. These methods exploit existing infrastructure, but fluorescent lights are energy inefficient, contain mercury and have reduced life cycle. All the methods above share the common idea that there exist a few static light fixtures, usually in the ceiling. Our work removes the need of static light fixtures and reduce the required LED luminaries to one. Our method also assumes *full mobility* with arbitrary Lambertian orders of the LED luminary, and no pre-recorded environmental/fingerprinting information is needed.

Table 4: Comparing previous works with this study

Study	Receivers	TXs	Evaluation	Calibration	Mobility
Lipro [18]	Single PD	Single LED	Empirical	Yes	Static (TX fixed)
Epsilon [9]	Single PD	Multiple LEDs	Empirical	Yes	Static (TX fixed)
Yin [21]	Single PD	Multiple LEDs	Theoretical	No	Static (RX fixed)
Yasir [20]	Single PD	Single/ Multiple LEDs	Empirical	No	Static (TX fixed)
Luxapose [8]	Single Image Sensor	Multiple LEDs	Empirical	No	Static (TX fixed)
This paper	Single PD	Single LED	Empirical	No	Dynamic (TX and RX can be mobile)

There has been some related work exploiting angle information. LiPro [18] is a system that uses a single light for localization. A smartphone, acting as receiver, has to be manually rotated around three axes, in a way similar to the calibration of a magnetic sensor. Another localization system is proposed in [21], describing a method using both angle-of-arrival principles and free-space attenuation of light signals to estimate the position of a mobile device. The method adopts multiple photodiodes installed on a ceiling acting as receivers, extending the proofs in [20]. Localization is done for a mobile device made of multiple LEDs fixed at different angles acting as a transmitter. The method is refereed to as *angle diversity transmitter* (ADT). Yasir et. al. [20] also exploit the Lambertian model of luminaries for localization. Both single or multiple reference points can be used to localize an object. The case of single fixed LED and multiple adjacent photodiodes has also been covered in [19], which estimates position using the difference of power received by multiple tilted optical receivers. However, in all the works described above there always exists reference points that are stationary. In this paper, we build on the works [18, 20, 21] by proposing, modeling and demonstrating a localization method with *nodes that can move freely* and with a single reference point (light). We proved that fully mobile systems require their own math and that, contrary to the simpler setup faced in indoor scenarios, the uniqueness of a solution is not guaranteed.

For fully mobile contexts, visible light that uses laser-ranging could be applied as well for distance computation. In particular, time-of-flight ranging sensors are gaining attention as a means to measure distances and being also available with small form factors. For instance, the recent VL53L1 [1] can accurately measure distances up to 4 meters. Economical laser lights have stringent safety regulations (Europe: EN 207, US: ANSI Z136) that limit the output power to only a few mW. In this work, we compute 2D relative position using standard LED sources, which are widely available.

9 CONCLUSION

We proposed a framework to compute the relative position of objects using LEDs. The method allows nodes to move freely in any direction and it works independently of the surrounding environment. Our approach requires a single light source and we derive close-form expressions to obtain unique localization solutions in most cases. The model is validated in different scenarios, and simulations are performed to obtain additional insights about the performance of our positioning method. Experimental results demonstrate the high accuracy of our model and also highlight the key factors affecting this accuracy. Currently, our model can compute the relative locations in a two-dimensional space and we envision that it can be applied in applications for manned and unmanned vehicles such as motorbikes and robots.

ACKNOWLEDGMENT

This work has been funded in part by the Madrid Regional Government through the TIGRE5-CM program (S2013/ICE-2919) and in part by "La Caixa international PhD program" fellowship.

A APPENDIX

A.1 Proof of Proposition 4.1

Proof. Since the TX does not rotate, we then have $\alpha^1_{\text{tx}} = \alpha^2_{\text{tx}}$ and $\psi_1 = \psi_2$. From Eq. (8), we have

$$\theta_i = \psi_1 - \pi - \alpha^1_{\text{tx}} + \alpha^i_{\text{rx}}, \quad i \in [1, 2] \tag{24}$$

Substituting Eq. (24) into Eq. (12), we get

$$\begin{cases} P^1_r = \frac{(m+1)A_{\text{RX}}}{2\pi d^2} \cos^m(\psi_1) \cdot \cos(\psi_1 - \alpha^1_{\text{tx}} + \alpha^1_{\text{rx}} - \pi) \cdot g_r + N \\ \quad = -\frac{(m+1)A_{\text{RX}}}{2\pi d^2} \cos^m(\psi_1) \cdot \cos(\psi_1 - \alpha^1_{\text{tx}} + \alpha^1_{\text{rx}}) \cdot g_r + N \\ P^2_r = \frac{(m+1)A_{\text{RX}}}{2\pi d^2} \cos^m(\psi_1) \cdot \cos(\psi_1 - \alpha^1_{\text{tx}} + \alpha^2_{\text{rx}} - \pi) \cdot g_r + N \\ \quad = -\frac{(m+1)A_{\text{RX}}}{2\pi d^2} \cos^m(\psi_1) \cdot \cos(\psi_1 - \alpha^1_{\text{tx}} + \alpha^2_{\text{rx}}) \cdot g_r + N \end{cases}$$

which leads to

$$\begin{aligned} \frac{P^1_r - N}{P^2_r - N} &= \frac{\cos(\psi_1 - \alpha^1_{\text{tx}} + \alpha^1_{\text{rx}})}{\cos(\psi_1 - \alpha^1_{\text{tx}} + \alpha^2_{\text{rx}})} \\ &= \frac{\cos(\psi_1 - \alpha^1_{\text{tx}})\cos(\alpha^1_{\text{rx}}) - \sin(\psi_1 - \alpha^1_{\text{tx}})\sin(\alpha^1_{\text{rx}})}{\cos(\psi_1 - \alpha^1_{\text{tx}})\cos(\alpha^2_{\text{rx}}) - \sin(\psi_1 - \alpha^1_{\text{tx}})\sin(\alpha^2_{\text{rx}})} \\ &= \frac{\cos(\alpha^1_{\text{rx}}) - \tan(\psi_1 - \alpha^1_{\text{tx}})\sin(\alpha^1_{\text{rx}})}{\cos(\alpha^2_{\text{rx}}) - \tan(\psi_1 - \alpha^1_{\text{tx}})\sin(\alpha^2_{\text{rx}})} \end{aligned} \tag{25}$$

From Eq. (25), we can easily derive the closed-form expression of ψ_1:

$$\psi_1 = \arctan\left(\frac{(P^1_r - N)\cos(\alpha^2_{\text{rx}}) - (P^2_r - N)\cos(\alpha^1_{\text{rx}})}{(P^1_r - N)\sin(\alpha^2_{\text{rx}}) - (P^2_r - N)\sin(\alpha^1_{\text{rx}})}\right) + \alpha^1_{\text{tx}}$$

Substituting the expression of ψ_1 into Eq. (8), we can easily obtain the expression of θ_2. □

A.2 Proof of Proposition 4.2

Proof. Since the RX does not rotate, we then have $\alpha^1_{\text{rx}} = \alpha^2_{\text{rx}}$ and $\theta_1 = \theta_2$. From Eq. (8), we now that

$$\theta_i = \psi_1 - \pi - \alpha^1_{\text{tx}} + \alpha^1_{\text{rx}}, \quad i \in [1, 2] \tag{26}$$

Substituting Eqs. (10) and (26) into Eq. (12), we get

$$\begin{cases} P_r^1 = \frac{(m+1)A_{\text{RX}}}{2\pi d^2}\cos^m(\psi_1)\cos(\psi_1-\alpha_{\text{tx}}^1+\alpha_{\text{rx}}^1-\pi)\cdot g_r + N \\ P_r^2 = \frac{(m+1)A_{\text{RX}}}{2\pi d^2}\cos^m(\psi_1+\alpha_{\text{tx}}^2-\alpha_{\text{tx}}^1)\cos(\psi_1-\alpha_{\text{tx}}^1+\alpha_{\text{rx}}^1-\pi)\cdot g_r \\ \qquad +N \end{cases}$$

which leads to

$$\begin{aligned} \frac{P_r^1-N}{P_r^2-N} &= \frac{\cos^m(\psi_1)}{\cos^m\left(\psi_1+\alpha_{\text{tx}}^2-\alpha_{\text{tx}}^1\right)} \\ &= \left(\frac{\cos(\psi_1)}{\cos(\psi_1)\cos\left(\alpha_{\text{tx}}^2-\alpha_{\text{tx}}^1\right)-\sin(\psi_1)\sin\left(\alpha_{\text{tx}}^2-\alpha_{\text{tx}}^1\right)}\right)^m \\ &= \left(\frac{1}{\cos\left(\alpha_{\text{tx}}^2-\alpha_{\text{tx}}^1\right)-\tan(\psi_1)\sin\left(\alpha_{\text{tx}}^2-\alpha_{\text{tx}}^1\right)}\right)^m \end{aligned} \tag{27}$$

From Eq. (27), we can easily derive the closed-form expression of ψ_1:

$$\psi_1 = \arctan\left(\frac{\cos\left(\alpha_{\text{tx}}^2-\alpha_{\text{tx}}^1\right)-\sqrt[m]{\frac{P_r^2-N}{P_r^1-N}}}{\sin\left(\alpha_{\text{tx}}^2-\alpha_{\text{tx}}^1\right)}\right) \tag{28}$$

Substituting Eq. (28) into Eq. (8), we can easily obtain the expression of θ_2, as given in Eq. (14). □

A.3 Proof of Proposition 4.3

Proof. In the full-rotation scenario, we have

$$\begin{cases} P_r^1 = -\frac{(m+1)A_{\text{RX}}}{2\pi d^2}\cos^m(\psi_1)\cos(\psi_1-\alpha_{\text{tx}}^1+\alpha_{\text{rx}}^1)\cdot g_r + N \\ P_r^2 = -\frac{(m+1)A_{\text{RX}}}{2\pi d^2}\cos^m(\psi_1+\alpha_{\text{tx}}^2-\alpha_{\text{tx}}^1) \\ \qquad\qquad \cos(\psi_1-\alpha_{\text{tx}}^1+\alpha_{\text{rx}}^2)\cdot g_r + N \end{cases}$$

which leads to

$$\frac{P_r^1-N}{P_r^2-N} = \frac{\cos^m(\psi_1)\cos(\psi_1-\alpha_{\text{tx}}^1+\alpha_{\text{rx}}^1)}{\cos^m(\psi_1+\alpha_{\text{tx}}^2-\alpha_{\text{tx}}^1)\cos(\psi_1-\alpha_{\text{tx}}^1+\alpha_{\text{rx}}^2)} \tag{29}$$

Let us first make some notations:

$$\begin{cases} b = \frac{P_r^1-N}{P_r^2-N} \\ c = \alpha_{\text{rx}}^1-\alpha_{\text{tx}}^1 \\ e = \alpha_{\text{tx}}^2-\alpha_{\text{tx}}^1 \\ h = \alpha_{\text{rx}}^2-\alpha_{\text{tx}}^1 \\ k = \cos e - \tan(\psi_1)\cdot\sin e \end{cases} \tag{30}$$

Then Eq. (29) becomes

$$\begin{aligned} b &= \frac{\cos^m(\psi_1)}{\cos^m(\psi_1+e)}\frac{\cos(\psi_1+c)}{\cos(\psi_1+h)} = \frac{1}{k^m}\frac{\cos c-\tan(\psi_1)\sin c}{\cos h-\tan(\psi_1)\sin h} \\ &= \frac{1}{k^m}\frac{\sin e\cos c-\cos e\sin c+k\sin c}{\sin e\cos h-\cos e\sin h+k\sin h} \\ &= \frac{1}{k^m}\frac{\sin(e-c)+k\sin c}{\sin(e-h)+k\sin h} = \frac{1}{k^m}\frac{\sin(\alpha_{\text{tx}}^2-\alpha_{\text{rx}}^1)+k\sin c}{\sin(\alpha_{\text{tx}}^2-\alpha_{\text{rx}}^2)+k\sin h} \end{aligned} \tag{31}$$

Let $x = \sin(\alpha_{\text{tx}}^2-\alpha_{\text{rx}}^1)$ and $y = \sin(\alpha_{\text{tx}}^2-\alpha_{\text{rx}}^2)$, then the above equation can be re-written as

$$b\cdot\sin(h)\cdot k^{m+1} + b\cdot y\cdot k^m - \sin(c)\cdot k - x = 0 \tag{32}$$

□

REFERENCES

[1] 2017. STmicroelectronics - VL53L1. (2017). http://www.st.com/content/st_com/en/products/imaging-and-photonics-solutions/proximity-sensors/vl53l1.html

[2] Ahmed Arafa, Sumant Dalmiya, Richard Klukas, and Jonathan F Holzman. 2015. Angle-of-arrival reception for optical wireless location technology. *Optics express* 23, 6 (2015), 7755–7766.

[3] Jean Armstrong, Y Sekercioglu, and Adrian Neild. 2013. Visible light positioning: A roadmap for international standardization. *IEEE Communications Magazine* 51, 12 (2013), 68–73.

[4] Christos Danakis, Mostafa Afgani, Gordon Povey, Ian Underwood, and Harald Haas. 2012. Using a CMOS camera sensor for visible light communication. *Proceedings of the IEEE Globecom Workshops* (2012).

[5] Trong-Hop Do and Myungsik Yoo. 2016. An in-depth survey of visible light communication based positioning systems. *Sensors* 16, 5 (2016), 678.

[6] Zabih Ghassemlooy, Wasiu Popoola, and Sujan Rajbhandari. 2012. *Optical wireless communications: system and channel modelling with Matlab®*. CRC press.

[7] Georg Kail, Patrick Maechler, Nicholas Preyss, and Andreas Burg. 2014. Robust asynchronous indoor localization using LED lighting. In *Proceedings of the IEEE International Conference on Acoustics, Speech and Signal Processing*. 1866–1870.

[8] Ye-Sheng Kuo, Pat Pannuto, Ko-Jen Hsiao, and Prabal Dutta. 2014. Luxapose: Indoor Positioning with Mobile Phones and Visible Light. In *Proceedings of the ACM Annual International Conference on Mobile Computing and Networking (MobiCom)*. 447–458.

[9] Liqun Li, Pan Hu, Chunyi Peng, Guobin Shen, and Feng Zhao. 2014. Epsilon: A Visible Light Based Positioning System.. In *Proceedings of the USENIX Symposium on Networked Systems Design and Implementation (NSDI)*. 331–343.

[10] Hui Liu, Houshang Darabi, Pat Banerjee, and Jing Liu. 2007. Survey of wireless indoor positioning techniques and systems. *IEEE Transactions on Systems, Man, and Cybernetics, Part C (Applications and Reviews)* 37, 6 (2007), 1067–1080.

[11] Dimitrios Lymberopoulos, Jie Liu, Xue Yang, Romit Roy Choudhury, Vlado Handziski, and Souvik Sen. 2015. A Realistic Evaluation and Comparison of Indoor Location Technologies: Experiences and Lessons Learned. In *Proceedings of the ACM International Conference on Information Processing in Sensor Networks (IPSN)*. 178–189.

[12] Kusha Panta and Jean Armstrong. 2012. Indoor localisation using white LEDs. *Electronics letters* 48, 4 (2012), 228–230.

[13] Anshul Rai, Krishna Kant Chintalapudi, Venkata N. Padmanabhan, and Rijurekha Sen. 2012. Zee: Zero-effort Crowdsourcing for Indoor Localization. In *Proceedings of the ACM Annual International Conference on Mobile Computing and Networking (MobiCom)*. 293–304.

[14] Jayakorn Vongkulbhisal, Bhume Chantaramolee, Yan Zhao, and Waleed S Mohammed. 2012. A fingerprinting-based indoor localization system using intensity modulation of light emitting diodes. *Microwave and Optical Technology Letters* 54, 5 (2012), 1218–1227.

[15] Qing Wang, Domenico Giustiniano, and Daniele Puccinelli. 2015. An Open-Source Research Platform for Embedded Visible Light Networking. *IEEE Wireless Communication* (2015).

[16] Qing Wang, Domenico Giustiniano, and Marco Zuniga. 2017. In Light and In Darkness, In Motion and In Stillness: A Reliable and Adaptive Receiver for the Internet of Lights. *IEEE Journal on Selected Areas in Communications (JSAC)* (2017).

[17] Zeyu Wang, Zhice Yang, Jiansong Zhang, Chenyu Huang, and Qian Zhang. 2015. Wearables Can Afford: Light-weight Indoor Positioning with Visible Light. In *Proceedings of the ACM Annual International Conference on Mobile Systems, Applications, and Services (Mobisys)*.

[18] Bo Xie, Shimin Gong, and Guang Tan. 2016. LiPro: light-based indoor positioning with rotating handheld devices. *Wireless Networks* (2016), 1–11.

[19] SH Yang, EM Jeong, and SK Han. 2014. Indoor positioning based on received optical power difference by angle of arrival. *Electronics Letters* 50, 1 (2014), 49–51.

[20] Muhammad Yasir, Siu-Wai Ho, and Badri N Vellambi. 2014. Indoor positioning system using visible light and accelerometer. *Journal of Lightwave Technology* 32, 19 (2014), 3306–3316.

[21] Liang Yin, Xiping Wu, and Harald Haas. 2015. Indoor visible light positioning with angle diversity transmitter. In *Proceedings of the IEEE Vehicular Technology Conference (VTC Fall)*. 1–5.

[22] Chi Zhang and Xinyu Zhang. 2016. LiTell: Robust Indoor Localization Using Unmodified Light Fixtures. In *Proceedings of the ACM Annual International Conference on Mobile Computing and Networking (MobiCom)*. 230–242.

[23] Shilin Zhu and Xinyu Zhang. 2017. Enabling High-Precision Visible Light Localization in Today's Buildings. In *Proceedings of the ACM Annual International Conference on Mobile Systems, Applications, and Services (Mobisys)*.